A Catalytic Intermediate and Several Flavin Redox States Stabilized by Folate-Dependent tRNA Methyltransferase from Bacillus subtilis

Djemel Hamdane, Vincent Guérineau, Sun Un, Béatrice Golinelli-Pimpaneau

A Catalytic Intermediate and Several Flavin Redox States Stabilized by Folate-Dependent tRNA Methyltransferase from *Bacillus subtilis*.[†]

Djemel Hamdane[‡*], Vincent Guérineau[$], Sun Un[∫] and Béatrice Golinelli-Pimpaneau[‡*]

[‡]Laboratoire d'Enzymologie et Biochimie Structurales, Centre de Recherche de Gif, CNRS, 91198 Gif-sur-Yvette, France,

[$]Institut de Chimie des Substances Naturelles, Centre de Recherche de Gif, CNRS, 91198 Gif-sur-Yvette, France and

[∫]Service de Bioénergétique Biologie Structurale et Mécanismes, CNRS, Institut de Biologie et Technologies de Saclay, CEA Saclay, 91191 Gif-sur-Yvette, France

[*] Corresponding author. Tel: 33 1 69 82 34 98, Fax: 33 1 69 82 31 29, E-mail: hamdane@lebs.cnrs-gif.fr

[*] Corresponding author. Tel: 33 1 69 82 42 35, Fax: 33 1 69 82 31 29, E-mail: beatrice.golinelli@lebs.cnrs-gif.fr

Running title: Several flavin reduced forms in TrmFO

keywords: RNA modification, methyltransferase, catalytic intermediate, flavin radical, 5-methyl-uridine, high field EPR, ENDOR, methylenetetrahydrofolate, flavoprotein, oxygen reactivity, spectroscopy.

[†]This work was supported in part by the CNRS, by a THYMET grant (PCV07_189094) from the Agence Nationale de la recherche (ANR-PCV) to B. G.-P. and by the Region Ile-de-France.

Abbreviations

tRNA, transfer ribonucleic acid; TrmFO, folate-dependent tRNA methyltransferase; $TrmFO_{TT}$, TrmFO from *Thermus thermophilus*; $TrmFO_{BS}$, TrmFO from *Bacillus subtilis*; CH_2THF, 5,10-methylenetetrahydrofolate; THF, tetrahydrofolate; FAD, flavin-adenine dinucleotide; FAD_{ox}, oxidized FAD; HFEPR, high field electron paramagnetic resonance; m^5U, 5-methyl-uridine; NAD(P)H, Nicotinamide adenine dinucleotide (phosphate); SHMT, serine hydroxymethyltransferase.

Abstract

The flavoprotein TrmFO catalyzes the C5-methylation of uridine 54 in the TΨC loop of tRNAs using 5,10-methylenetetrahydrofolate (CH_2THF) as a methylene donor and FAD as a reducing agent. Here, we report biochemical and spectroscopic studies that unravel the remarkable capability of *Bacillus subtilis* TrmFO to stabilize, in the presence of oxygen, several flavin reduced forms, including an FADH• radical, and a catalytic intermediate endowed with methylating activity. The FADH• radical was characterized by high field EPR and ENDOR spectroscopies. Interestingly, the enzyme exhibited tRNA methylation activity in the absence of both added carbon donor and external reducing agent, indicating that a reaction intermediate, containing presumably CH_2THF and FAD hydroquinone, is present in freshly purified enzyme. Isolation by acid treatment, under anaerobic conditions, of noncovalently bound molecules, followed by mass spectrometry analysis, confirmed the presence in TrmFO of non-modified FAD. Addition of formaldehyde to the purified enzyme protects the reduced flavins from decay by probably preventing degradation of CH_2THF. The absence of air-stable reduced FAD species during anaerobic titration of oxidized TrmFO, performed in the absence or presence of added CH_2THF, argues against their thermodynamic stabilization but rather implicates their kinetic trapping by the enzyme. Altogether, the unexpected isolation of a stable catalytic intermediate suggests that the flavin-binding pocket of TrmFO is a highly insulated environment, diverting the reduced FAD present in this intermediate from uncoupled reactions.

Maturation of transfer RNA (tRNA), which is necessary for its correct functioning during protein translation, requires extensive processing including a large number of chemical modifications of nucleotides. For instance, the C^5-methylation of uridine, invariably found at position 54 (m^5U54) in the TΨC loop of tRNA of almost all living cells, is one of the modifications important for maintaining the tertiary structure of tRNA (*1*). In most Gram positive bacteria, 5,10-methylenetetrahydrofolate (CH_2THF) serves as the carbon donor in the enzyme-catalyzed reaction (*2*). The folate-dependent methylation reaction requires a two-electron reduced FAD (FAD hydroquinone), and tetrahydrofolate (THF) is released as product (*2, 3*) (Figure 1A). The role of the FAD hydroquinone as the reducing agent of the methylene-U54-tRNA intermediate was established in the *Streptococcus faecalis* enzyme by showing direct tritium incorporation from labeled 5-[^{3}H]5-deaza-$FMNH_2$ into the methyl moiety (*3*). This experiment was also indicative of a hydride transfer rather than a radical mechanism. A mechanism was thus proposed for the reaction, in which CH_2THF donates a methylene group to the C5 atom of U54 in tRNA, and then the resulting exocyclic methylene-U54 intermediate is reduced by a hydride anion deriving from the FAD hydroquinone to form m^5U54-tRNA (*3*). Nonetheless, the nature of the electron donor to FAD *in vivo* remained unclear. The gene responsible for this class of methyltransferases, which encodes an FAD-containing flavoprotein (TrmFO), was discovered afterwards (*4*).

The structure of *Thermus thermophilus* TrmFO ($TrmFO_{TT}$) was recently solved alone and in complex with tetrahydrofolate or glutathione (*5*) (Figure 1B). To evaluate the methylation activity of $TrmFO_{TT}$ and several mutants, a new *in vitro* test was designed, in which the CH_2THF substrate required for the TrmFO reaction is directly generated as a

metabolic product of serine hydroxymethyltransferase (SHMT) using radio-labeled [^{14}C]Ser and THF as substrates of SHMT. Methylation activity of $TrmFO_{TT}$ was detected with this assay in the absence of NADPH. The authors interpreted this unexpected result by the presence of an FAD reduced state in purified $TrmFO_{TT}$.

Reduced FAD can assume two different active redox states, the one electron-reduced semiquinone radical form (FADH• or its N(5) deprotonated form FAD•-) and the fully reduced hydroquinone form ($FADH_2$ or its N(1) deprotonated form FADH-) (Scheme 1). Therefore, the flavin moiety can participate in redox reactions as either one- or two-electron mediator depending on its chemical environment. Only certain types of flavoproteins are able to specifically stabilize the flavin radical, which is elusive when not bound to an enzyme. In some flavoenzymes such as DNA photolyase (*6*) or cytochrome P450 reductase (*7, 8*), the paramagnetic flavin radicals have been identified as air-stable catalytic intermediates. Conversely, the flavin hydroquinones generated in enzyme active sites are generally extremely air-sensitive (*9*).

The structure of $TrmFO_{TT}$ in complex with THF shows that the flavin is located in a well-insulated environment since its isoalloxazine ring is sandwiched between the THF pteridine ring and several residues of the protein (Figure 1B). To know whether the environment of the TrmFO binding site might be prone to shelter a catalytically active reduced form of the FAD cofactor from air oxidation, we carried out a thorough spectroscopic characterization of TrmFO from *Bacillus subtilis* ($TrmFO_{BS}$), which we succeeded to produce in high amounts (*10*). This study is one of the primordial steps towards the elucidation of the enzymatic mechanism. We report here the ability of purified $TrmFO_{BS}$ to stabilize the protonated semiquinone FADH• and a catalytic

intermediate containing most likely both methylenetetrahydrofolate and an FAD reduced form. Our experiments indicate that $TrmFO_{BS}$, in the absence of tRNA, maintains an insulated active site that locks up the methyl donor and protects the reduced forms of the flavin from deleterious oxidative reactions.

Experimental procedures

Protein preparations. Recombinant N-terminus $(His)_6$-tagged $TrmFO_{BS}$ was expressed and purified as reported (*10*). The protein purity was > 95% as judged by SDS-PAGE. The protein was concentrated to ≈ 500-800 μM in 50 mM Tris-HCl pH 7.8, 150 mM NaCl, 10 % (v/v) glycerol and stored at -80°C.

UV-visible Spectroscopy. All UV-visible absorption spectra were recorded from 250 to 750 nm on a Cary 50 spectrophotometer (Varian) at room temperature. For anaerobic experiments, the buffer and samples were made oxygen-free by purging several times with argon and nitrogen.

EPR and ENDOR spectroscopy. The 285 GHz HFEPR spectrometer has been described in detail elsewhere (*11*). Field calibration was based on a small Mn(II)-doped MgO (Mn:MgO) standard sample (g=2.000101) mounted immediately above the frozen sample. Home written computer programs were used for the simulations of the HFEPR spectra. High-field 95 GHz Davies ENDOR measurements were carried out on a Bruker E680 95 GHz spectrometer equipped with a Bruker 400 mW power upgrade, an Oxford Instruments CF935P helium flow cryostat and an Amplifier Research 500A250A radio-frequency amplifier. A selective inversion of the electron spin was achieved using a 200

ns microwave pulse, followed by a 12 (π/2) and 24 ns (π) pulses for echo detection. A 5 μs radio-frequency pulse was used to pump the nuclear spins.

Kinetics of m^5U54 formation. The kinetic rate of tRNA methylation by TrmFO was determined, as described previously (*10, 12*), using an *E. coli* [α-^{32}P]UTP-labeled $tRNA^{Ala1}$ transcript. 50–100 fmol of [α-^{32}P]$tRNA^{Ala1}$ was incubated at 37°C under aerobic conditions in a 50 μL reaction mixture containing 50 mM N-(2-hydroxyethyl) piperazine-N-(2-ethanesulfonic acid)–Na buffer (HEPES–Na, Sigma), pH 7.5, 100 mM ammonium sulfate, 0.1 mM EDTA, 25 mM mercaptoethanol (Promega) and 20% glycerol in the presence and absence of 0.5 mM NADH (Sigma), 0.5 mM (6R,S)-N5,N10-CH_2H_4PteGlu–Na_2 (methylenetetrahydrofolate). The reaction was started by the addition of 0.2 μM purified TrmFO (~0.1 μM based on FAD content). After various incubation times, the tRNA product was phenol extracted and digested with nuclease P1 (Roche), which generates 5'-nucleoside monophosphates. The hydrolysate was analyzed by 2D thin-layer chromatography on cellulose plates (Machery Nagel). The amount of m^5U formed per tRNA molecule was determined by measuring the radioactivity in the TLC spots using a PhosphorImager screen and quantification with the ImageQuant software.

Stoichiometry of tRNA methylation quantified by MALDI-MS. MALDI mass spectrometry was used to estimate the stoichiometry of the methylation reaction catalyzed by $TrmFO_{BS}$ by analyzing the relative amount of modified and non-modified tRNA fragment obtained after RNAase A treatment. *E. coli* $tRNA^{Asp}$ transcript (10 μM) was incubated for 1 hour at 37˚C with 0.1, 1, 5 or 10 molar equivalent of purified $TrmFO_{BS}$ (calculated based on flavin content) under aerobic conditions in 50 μL 50 mM HEPES–Na pH 7.5, 100 mM

ammonium sulfate, 0.1 mM EDTA, 25 mM mercaptoethanol (Promega), 20% glycerol. The reaction was stopped by adding 200 µL of phenol/chloroform/isoamyl alcohol (25/24/1, v/v/v) pH 4.5, and the tRNA product in the aqueous phase was extracted by centrifugation at 10,000 g for 5 min. The tRNA was then precipitated with 350 µL of cold ethanol in the presence of 60 mM sodium acetate pH 5.4, and incubated for at least 1 hour at -20˚C. The tRNA pellet, recovered after centrifugation at 10,000 *g* for 1 hour at 4˚C, was dried and dissolved in 15 µL of water. Then, the tRNA was digested overnight at 37˚C with 0.2 µg of pancreatic bovine ribonuclease A (Fermentas). This hydrolysate (1 µL) was mixed with 9 µL 2,5-dihydroxybenzoic acid matrix (20 mg/mL in MeOH/H_2O 1/1; Sigma-Aldrich, Saint Quentin Fallavier, France), and 1 µL of this mixture was spotted on the MALDI plate and air-dried. The Perseptive Voyager DE-STR MALDI-TOF mass spectrometer (Applied Biosystems, Les Ulis, France), equipped with a 337-nm pulsed nitrogen laser (20 Hz) and a Acqiris® 2 GHz digitizer board, was externally calibrated. Mass spectra were obtained in the reflectron positive ion mode with an accelerating voltage of 20 kV, a grid voltage corresponding to 62 % of accelerating voltage and an extraction delay time of 150 ns. The laser intensity was set just above the ion generation threshold to obtain peaks with the highest possible signal-to-noise ratio without significant peak broadening. The data were processed using DataExplorer 4.4 (Applied Biosystems). The molar ratio of formed m^5U was determined by integrating the peaks corresponding to the methylated versus non-methylated GGGGU fragment.

Extraction and identification of non-modified FAD present in TrmFO$_{BS}$ by MALDI-TOF-MS. Aliquots of 20 µL of $TrmFO_{BS}$ (700 µM) were sealed in microtubes and deoxygenated by flushing with nitrogen for 30 min at 4°C. After 1:10 dilution of the

samples with deoxygenated water, the proteins were precipitated by addition of 10 μL of 3.7% HCl under stringent anaerobic conditions and removed after incubation on ice for 20 min by centrifugation at 13,000 x g during 15 min. The resulting yellowish supernatants were transferred anaerobically into new deoxygenated vials before mass measurements. This extract (1 μL) was added to 9 μL of 2,5-dihydroxybenzoic acid matrix, and 1 μL of this mixture was subsequently spotted on the MALDI plate and air-dried. To ensure the absence of methylated flavin in $TrmFO_{BS}$, commercial free FAD and synthesized N(5)-CH_3-FAD, treated in the same conditions as described above for the protein, were used as controls. N(5)-CH_3-FAD was synthesized by incubating FAD (50 μM), stoichiometrically reduced with sodium dithionite, with 20-fold excess methyl-iodide in 50 mM potassium phosphate pH 8 under anaerobic conditions. The reaction mixture was incubated overnight at room temperature, then analyzed by MALDI-MS under the conditions described above for tRNA methylation.

Fluorescence spectroscopy. Fluorescence spectra of $TrmFO_{BS}$ (2 to 5 μM) were recorded on a Cary Eclipse fluorescence spectrophotometer (Varian) with excitation and emission slit widths of 5 nm. When the flavin fluorescence was excited at 370 and 450 nm, emission was monitored from 380 to 700 nm or 465 to 700 nm, respectively. The excitation spectra were recorded by setting the λ_{em} at the maximum peak observed in the emission spectrum.

Oxidation kinetics of the air-stable reduced states. Oxidation kinetics of the reduced flavins were followed spectrophotometrically by recording the whole spectrum from 750 to 250 nm after mixing 20-30 μM $TrmFO_{BS}$ with 50 mM oxygenated potassium phosphate buffer, 150 mM NaCl, 10% glycerol at pH 7 and pH 8 in a 1 cm pathlength

quartz cuvette. The oxidation of $TrmFO_{BS}$ was performed under different concentrations of oxygen (atmospheric pressure (1 atm) and 80 μM [O_2]). To test the effect of formaldehyde on the oxidation kinetics, 700 μL of 50 mM oxygenated potassium phosphate buffer, 150 mM NaCl, 10% glycerol at pH 8, containing 10 mM formaldehyde, was equilibrated with 1 atm O_2 at 30˚C in a 4x10 mm quartz cuvette, and the oxidation reaction was started after the addition of freshly purified $TrmFO_{BS}$ (~20 μM final).

Anaerobic titration and auto-oxidation of fully reduced $TrmFO_{BS}$. Air-oxidized $TrmFO_{BS}$ (~10 μM) was reduced by titrating with sodium dithionite in 1 mL deoxygenated buffer containing 10% glycerol. Upon completion of the anaerobic titration, the reduced protein was exposed to room air and the absorbance change occurring during autoxidation was recorded in the single wavelength mode at 450 and 595 nm.

Results

Identification and characterization by high field EPR and ENDOR spectroscopies of an air-stable FADH• radical in $TrmFO_{BS}$. Immediately after isolation, the $TrmFO_{BS}$ protein was green. The UV-visible absorbance spectrum of freshly purified TrmFO at pH 8 is consistent with the presence of an air-stable protonated form of FAD radical (FADH•), as evidenced by the broad shoulder observed from 595 to 650 nm (Figure 2, continuous line) (*13*). The amount of the FADH• radical was found to be preparation dependent and varied between 20 and 39%. After 20 h incubation at room temperature, the spectrum changed to that of fully oxidized FAD (FAD_{ox}) (Figure 2, dashed line).

To further characterize the FADH• radical environment, high field EPR and ENDOR spectra of frozen $TrmFO_{BS}$ were measured. The 10K 285 GHz HFEPR spectrum at pH 8 is shown in Figure 3A. The overall shape of the spectrum is dominated by the electronic Zeeman interaction, the magnitude of which is defined by the three principal g-tensor values ($g_x \geq g_y \geq g_z$ by convention, Scheme 1). At this observation frequency, the magnetic-fields corresponding to each of these three values were resolved. The spectra were fitted to a spin-Hamiltonian containing the electronic Zeeman interaction and three hyperfine interactions, two to ^{14}N nuclei and one to a proton to model the interaction of the electron spin of the radical with N(5), N(10) and H(5) (Table 1A). The g-values are reported in Table 1B along with values of the FAD radicals in glucose oxidase from *Aspergillus niger* (*14*) and NADH:quinone reductase from *Vibrio cholerae* (*15*). Density Functional Theory was used on a supramolecular complex model, in which a neutral flavin radical is embedded in a dielectric medium (ε=20) and the N(5)H makes a hydrogen-bond to a methyl thiol molecule to mimic the interactions observed in the $TrmFO_{TT}$ crystal structure (Figure 1B) (*5*). This calculation yielded g-values that were 0.0006 lower than the experimental values but similar to those of flavin radicals (Table 1B).

The Davies pulse 95 GHz proton ENDOR spectrum was obtained at a magnetic field corresponding to the g_y-value (Figure 3B). Such spectra display a series of peaks symmetrically displaced about the proton Zeeman frequency. For each proton, there are two resonances with frequencies $\nu_{ENDOR}=\nu_{Zeeman}\pm A(\theta,\phi)/2$, where $A(\theta,\phi)$ is the hyperfine coupling, the value of which depends on the orientation of the flavin molecule relative to the applied magnetic field and ν_{Zeeman} is the nuclear Zeeman frequency (about 143 MHz

in our case). A detailed analysis of the $TrmFO_{BS}$ ENDOR spectra will be presented elsewhere. Here we focus on the tensorial line shapes in the region of the ENDOR spectrum flanking the central matrix-ENDOR signal, arising from hyperfine couplings of the H(1'), H(6) and H(8α) protons with the unpaired electron spin (Scheme 1, Figure 3B). The H(6) hyperfine coupling of 5.0 MHz is consistent with reported values for other flavoproteins. As pointed out by Schleicher and coworkers (*16*), the size of the H(8α) hyperfine coupling is a diagnostic for the protonation state of the flavin radical: ~ 7.0 MHz for neutral FADH• and ~10.5 MHz for the anionic FAD•-. The TrmFO H(8α) hyperfine coupling value of 7.2 MHz indicates a neutral radical, as expected from the optical data, and rules out the presence of FAD•-. In previous reported spectra (*16-18*), the broad features beyond ±10 MHz (Figure 3B) were assigned to the N(5) proton. In our case, the broad ENDOR resonance that extends from 8 to 11.5 MHz (and -8 to -11.5 MHz, as indicated by the vertical dashed line in Figure 3B) likely arises from the ribityl H(1') and is dominated by an isotropic hyperfine coupling of 19.5 MHz. This value is higher than the values that have been previously reported for other flavoenzyme systems and different from the previously reported ENDOR spectrum of the N(5) proton that was highly anisotropic (*16*). This indicated that the dihedral angle of H(1') relative to the ring-plane was larger and closer to perpendicular than in these other FADH• radicals. From the approximately ring-perpendicular position of the FAD C1'-C2' bond in the crystal structure of $TrmFO_{TT}$, one would have expected the two H(1') protons to have a dihedral angle of 30º relative to the ring-plane. This appears not to be the case. The orientation dependence of this and other resonances will be further detailed elsewhere.

A competent methylating intermediate is present in freshly purified TrmFO$_{BS}$. The kinetics of tRNA methylation by TrmFO$_{BS}$ were examined using [α-^{32}P]-labeled *E. coli* tRNA^{Ala1} under single-turnover conditions. As shown in Figure 4A, TrmFO$_{BS}$ methylates tRNA efficiently. The time course of the methylation reaction could be fitted to a mono-exponential with a rate constant of ~ 0.4/min. Similar to the findings of Nishimasu et al. for TrmFO$_{TT}$ (*5*), TrmFO$_{BS}$ did not require exogenous NAD(P)H for activity and the rate was independent of added NAD(P)H up to 1 mM, the maximum concentration tested. In addition, as reported previously (*4*), the pre-steady state methylation activity of TrmFO$_{BS}$ was detected in the absence of CH_2THF. However, the increase of methylation rate when adding CH_2THF, reported by Urbonavicius et al. (*4*), was not observed. Surprisingly, the full oxidation of the air-stable reduced form of TrmFO$_{BS}$ upon air exposure led to an irreversible inactivation of the protein since the presence of a large excess of NAD(P)H and CH_2THF did not restore any methyltransferase activity.

Since external CH_2THF and reducing agent were not required for tRNA methylation under conditions where enzyme is in great excess over tRNA, the logical implication is that a catalytically competent intermediate, containing both CH_2THF and an FAD hydroquinone, was already present inside the active site of a significant enzyme fraction. In this case, the FAD hydroquinone would be well protected from solvent because the strong oxidant ferricyanide did not disrupt methylation.

Estimation of the amount of the catalytically competent intermediate by mass spectrometry. To estimate the amount of air-stable catalytic intermediate locked up in purified TrmFO$_{BS}$, the stoichiometry of the methylation reaction was analyzed using mass spectrometry. Enzyme and *E. coli* tRNA^{Asp} were mixed in 10:1, 1:1 and 1:10 ratios

(Figure 4B). After reaction, the methylated tRNA product was digested with RNAse A, which cleaves after C and U and generates 3'-phosphate nucleosides. The generated fragments were analyzed by MALDI-MS. Fragments (*m/z* = 1705.2, 1719.2) coincide with the expected masses of non- and monomethylated fragments derived from GGGGU corresponding to the sequence from G50 to U54 in *E.coli* $tRNA^{Asp}$. The experiment where the tRNA:enzyme ratio is 10:1, and the control in the absence of $TrmFO_{BS}$, display only the nonmethylated fragment (Figure 4B). Increasing the amount of enzyme in the assay to 1:1 and 1:10 tRNA:enzyme ratios results in the decrease of the nonmethylated fragment with concomitant increase of the methylated fragment. Addition of 0.5 mM NAD(P)H and CH_2THF had no effect on the peaks distribution. These results confirm that $TrmFO_{BS}$ does not need exogenous NAD(P)H and CH_2THF for catalyzing the initial formation of m^5U54 but show that the addition of these compounds is not sufficient for enzymatic turnover. The ratio between the peaks areas of the nonmethylated and methylated fragments allows us to estimate the stoichiometry of the methylation reaction and thus the fraction of catalytic intermediate present in the purified enzyme. When $TrmFO_{BS}$ was mixed with an equimolar amount of tRNA, 17% of U54-tRNA was methylated, indicating that at least the same proportion of catalytic intermediate is present in purified $TrmFO_{BS}$. On the other hand, in the presence of a 5 or 10-fold excess $TrmFO_{BS}$, almost all U54 was modified (Figure 4B).

Isolation and identification of non-modified FAD in freshly purified $TrmFO_{BS}$. Because the optical spectrum of the freshly purified enzyme (Figure 2) is reminiscent of an alkylated FAD derivative, the nature of the catalytic intermediate was addressed by analyzing small molecules that co-purified with $TrmFO_{BS}$ by MALDI-TOF MS after

acidic treatment under anaerobic conditions. As shown in Figure 5, the mass spectrum shows that a unique molecule has been released from TrmFO and is thus not covalently bound to the protein. The highest peak in the mass profile is centered at 787.15 Da and corresponds to free FAD. This result indicates that the released FAD does not bear any chemical modification. In contrast, the mass profile of the free FAD modified by methyl-idodide, which was used as control, displays, in addition to free FAD, peaks that are attributable to mono-methylated FAD, most likely N(5)-CH_3-FAD, indicating that the methyl group is not labile in these conditions. Taken together, these results confirm that N(5)-methylated flavin cannot constitute the catalytic intermediate observed in the freshly isolated enzyme.

No other peaks attributable to CH_2THF were observed in the mass spectrum of $TrmFO_{BS}$ after acidic treatment under anaerobic conditions. Similarly, other attempts to extract the cofactor from $TrmFO_{BS}$ by heating or by using chaotropic denaturants (urea, guanidinium chloride) were all unsuccessful in identifying the presence of CH_2THF (data not shown).

Identification and characterization of additional flavin species in the freshly purified $TrmFO_{BS}$. Beside FADH•, the UV-visible spectrum of freshly purified $TrmFO_{BS}$ displays an unusual high and broad absorption peak around 380 nm (Figure 2). This spectral component slowly vanishes while a peak at 450 nm, characteristic of oxidized FAD, concomitantly appears. After treatment with a large excess of ferricyanide, the greenish purified $TrmFO_{BS}$ turned lightly yellow but the peak at 380 nm was not affected (Figure 6). The color of the sample indicates that FADH• was oxidized and that the red-colored FAD•- was absent, eliminating both radicals as the source of the peak absorbing at 380

nm. The spectrum of the flavin species absorbing at 380 nm was extracted from the spectrum of $TrmFO_{BS}$ treated by ferricyanide (Figure 6) by subtracting the contribution of FAD_{ox}. The obtained spectrum displays a poorly resolved line shape below 340 nm associated with a relatively broad absorption peak at 379 nm.

To further characterize the air-stable FAD species absorbing at 380 nm, we examined the steady-state excitation and emission fluorescence spectra of the enzyme (Figure 7). The excitation spectrum of $TrmFO_{BS}$ recorded at λ_{em} of 528 nm exhibits the same electronic transitions that were observed in the absorption spectrum, with peaks at 370 and 450 nm (Figure 7A), whereas the excitation spectrum at λ_{em} of 450 nm shares very close similarity with the calculated absorbance spectrum shown in Figure 6. This result indicates that both the observed fluorescence and absorbance relate to the same chromophore(s) species and validates the calculated spectrum (Figure 6). Upon excitation at 450 nm, a weak fluorescence emission peak at 528 nm characteristic of FAD_{ox} was observed. This peak arises from properly bound flavin and not from traces of free FAD_{ox}. Indeed, when the protein was denatured with 8 M urea, its intensity was increased about 20-fold (Figure 7B), whereas a strong fluorescence emission peak was observed at 530 nm upon excitation at 370 nm, showing the subsequent release and oxidation of the air-stable reduced flavin.

Characterization of the stability of the reduced FAD species observed in $TrmFO_{BS}$. The stability of the different reduced redox states present in the freshly purified protein was assessed by measuring the kinetics of flavin oxidation under different concentrations of molecular oxygen (Figure 8). The oxidation of FADH• was specifically determined by following the disappearance of the absorbance at 595 nm while the oxidation of the other

species was monitored at 450 nm. All the air-stable reduced forms are slowly converted to the oxidized state. The time-dependent transition between the reduced FAD species and oxidized FAD exhibits two isosbestic points, 348 and 503 nm (Figure 8A) and is also pH dependent (data not shown). At 30˚C, the oxidation kinetics are monophasic, whichever wavelength is monitored (Figure 8B), and are moderately affected by the oxygen concentration. Surprisingly, all the reduced states are oxidized at the same rate and oxygen is not the major factor contributing to their decay. Indeed, increasing the oxygen concentration from ~80 μM to 1 atm (~ 10 fold) accelerates the rate from 0.08/hr to 0.15/hr for the unknown reduced FAD and from 0.1/hr to 0.16/hr for FADH•. To examine whether the gradual degradation of presumably locked up CH_2THF could have enabled molecular oxygen to diffuse toward the enzyme active site, the stability of the reduced species was determined in the presence of formaldehyde, a molecule known to protect CH_2THF from decomposition into THF and formaldehyde. As observed in Figure 8B, the reduced states are drastically stabilized by formaldehyde since the rates determined at 450 nm and 595 nm decrease to 0.009/hr and 0.03/hr, respectively. These results indicate that CH_2THF protects the air-stable reduced flavins from oxidation and suggest that its degradation constitutes the rate-limiting step in the autooxidation reaction of $TrmFO_{BS}$.

Anaerobic titration of oxidized $TrmFO_{BS}$ reveals that the air-stable reduced flavins are not thermodynamically relevant. To determine whether the one- and two-electron reduced states of FAD are thermodynamically relevant in $TrmFO_{BS}$, the air-oxidized $TrmFO_{BS}$ enzyme was first titrated with dithionite (Figure 9A). The reduction of the enzyme caused a decrease in the intensity of the visible absorption bands with the loss of

the fine structure in the peak centered at 450 nm without the concomitant formation of a broad band between 595 and 650 nm characteristic of FADH•. Additionally, the unique isosbestic point near 334 nm indicates a transition between two chemical species, oxidized and reduced $TrmFO_{BS}$. These observations indicate that the reduction of oxidized flavin proceeds directly to the FAD hydroquinone without transient stabilization of the FADH• radical. The shape of the resulting 2-electron reduced FAD spectrum is similar to that of classical flavin hydroquinones, and is clearly distinct from that of the air-stable reduced FAD species stabilized by $TrmFO_{BS}$ (Figure 6). Upon air exposure, the flavin hydroquinone generated by dithionite titration was oxidized so rapidly that it could not be followed spectrophotometrically. In addition, no signal attributable to stable FADH• was detected, indicating that the hydroquinone is converted directly to fully oxidized FAD. This difference in sensitivity to air oxidation of the hydroquinone formed upon dithionite titration, compared to reduced FAD species locked up in freshly purified $TrmFO_{BS}$, could be due to the loss of CH_2THF. To evaluate this possibility, the anaerobic titration of $TrmFO_{BS}$ was repeated in the presence of chemically synthesized CH_2THF (data not shown). The resulting FAD hydroquinone was still oxidized rapidly, demonstrating that exogenous CH_2THF is unable to protect the reduced flavin from air oxidation.

Discussion

Characterization of the electronic structure of the neutral flavin radical stabilized by $TrmFO_{BS}$. After the pioneering biochemical work of Delk et al. on the *Streptococus faecalis* TrmFO enzyme (*3*), it was subsequently confirmed that the *B. subtilis* and *T.*

thermophilus TrmFO recombinant proteins isolated from *E. coli* methylate tRNA using CH_2THF and NAD(P)H as the carbon donor and the reducing agent of the FAD, respectively (*4, 5*). In the present paper, we characterized the uncommon properties of the $TrmFO_{BS}$ flavin. Our spectroscopic studies have revealed the ability of $TrmFO_{BS}$ to stabilize both the FADH• radical and at least one other reduced FAD species under aerobic conditions. UV-visible, high field EPR and ENDOR spectra are consistent with the stabilization of a neutral protonated FADH• radical but not of the anionic form FAD•- . The absorbance of FADH• in the 595 to 650 nm region is somehow red-shifted compared to most flavoprotein systems (*13*). Such variation was also observed in photolyase and interpreted as a stronger hydrogen bonding interaction between FADH• and its immediate vicinity (*19-21*).

Although stabilization of flavin radicals is commonly encountered in other flavoprotein systems such as photolyase, cryptochromes, flavodoxins, P450 reductase (*8, 22-24*), the g-values determined by HFEPR at 285 GHz for the $TrmFO_{BS}$ FADH• radical are unusual. Indeed, the TrmFO g-values, although consistent with those previously reported for FADH• or FAD•- radicals, are unique in that all three g-values are shifted to higher values (*14, 15*). In particular, the g_z value of 2.00258 is well above the free electron g-value (2.00232) despite the fact that planar π-type radicals (delocalization of the p_z orbital network) are theoretically expected to have a g_z value lower than the free electron value. To understand how the protein environment affects the FADH• radical g-values, we calculated theoretical g-values using Density Functional Theory based on the known $TrmFO_{TT}$ crystal structure (*5*), in which the thiol side chain of Cys51 is hydrogen bonded to the FAD N(5) atom (Figure 1B). The calculated g-values were more consistent

with those of previously reported flavin radicals (Table 1B) than with the experimental g-values obtained for $TrmFO_{BS}$, indicating that our minimal computational model was not sufficient to account for the unusual large g-values of $TrmFO_{BS}$ and high g_z value. More complex models are currently being investigated. In contrast to the EPR results, the proton hyperfine couplings of the $TrmFO_{BS}$ radical determined from the 95 GHz proton ENDOR spectrum ENDOR spectrum were entirely consistent with those previously reported for FADH• radicals in other flavoproteins (*18*), indicating that the unpaired spin density distribution of the $TrmFO_{BS}$ radical and its electronic structure were the same as in the other FADH• radicals. The apparent contradictory view, given by the g-values and proton hyperfine coupling, would suggest that the former may be more sensitive to external electronic interactions. This behavior was also observed in the case of tyrosyl radicals (*25*). The unusual $TrmFO_{BS}$ radical g-values may be indicative of interaction with the nearby presumed CH_2THF molecule.

CH_2THF is most likely the carbon donor present in the catalytic methylating intermediate observed in freshly purified enzyme. Interestingly, we confirm here, as noticed previously by Urbonavicius et al. (*4*), that $TrmFO_{BS}$ is able to catalyze the formation of m^5U54 in the absence of exogenous CH_2THF. This result was obtained both under pre-steady-state conditions using [α-^{32}P]-labeled tRNA or with tRNA and enzyme in equimolar ratio using mass spectrometry (Figure 4). This observation suggests that the methyl donor co-purifies with the enzyme, although attempts to isolate this molecule from the purified enzyme after heat, urea or acidic treatment and to characterize it by mass spectrometry remained unsuccessful. It is possible that the folate compound precipitates with the protein under our assay conditions owing to its polyglutamate chain and/or its high

affinity for the enzyme. Sequestration of folate derivatives by proteins is quite common and has been reported in several enzymes including photolyase (*26*) and MnmE (formely named TrmE), a folate-dependent tRNA-modification enzyme (*27*). This phenomenon is explained by the high affinities exhibited by these proteins for their respective folate derivatives (*28-30*). In $TrmFO_{TT}$, the tRNA methylation reaction was carried out in the presence of SHMT in order to produce CH_2THF (*5*). It was hypothesized that $TrmFO_{TT}$ could form a channeling complex with SHMT to facilitate m^5U54 biosynthesis. If such a protein complex exists in the cell, it could also help to insulate the reduced FAD. The observation that no methylated tRNA product was synthesized by $TrmFO_{BS}$ in the presence of CH_2THF and NAD(P)H under steady state conditions is in agreement with the likely existence of a protein partner that would channel CH_2THF *in vivo*. Several enzymes are known to channel folate derivatives (*29*), such as the bifunctional enzymes thymidylate synthase-dihydrofolate reductase from *Leishmania major* (*31*) and *Toxoplasma gondii* (*32*), and human methylenetetrahydrofolate dehydrogenase/cyclohydrolase domain (*33*).

By examining the crystal structure of $TrmFO_{TT}$ (*5*), it can be noticed that there is not enough room to accommodate the three substrates together, namely NAD(P)H, CH_2THF and tRNA with U54 flipped into the active site. Therefore, as proposed for methylenetetrahydrofolate reductase (*34*), the only other known enzyme in which THF stacks with FAD besides TrmFO, the hydride may be transferred from the NAD(P)H to FAD before the binding of CH_2THF and tRNA, which is consistent with the sequestration of both an FAD reduced form and CH_2THF in the active site of $TrmFO_{BS}$. In the X-ray structure of $TrmFO_{TT}$ in complex with the folate product THF, the latter binds to the

enzyme on the solvent accessible *re*-face of the FAD moiety (Figure 1B) (*5*), thereby restricting access to the reactive N(5) atom of the FAD isoalloxazine. Interestingly, in methylenetetrahydrofolate reductase, the pterin ring of methyltetrahydrofolate is stacked against FAD in a similar orientation, which is favorable for hydride transfer (*34*).

Identification of reduced FAD species present in freshly purified $TrmFO_{BS}$ and characterization of their stability. The presence of a stable FAD radical suggested the intriguing possibility that the $TrmFO_{BS}$ methylation could proceed via a radical mechanism. Upon ferricyanide treatment, the FADH• radical was oxidized while the other reduced FAD states were preserved (Figure 6). However, oxidation of $TrmFO_{BS}$ by ferricyanide did not affect activity (data not shown), indicating that the radical is unlikely to be a catalytically competent intermediate in the reduction of C5-methylene-U54-containing tRNA. According to the proposed catalytic mechanism of TrmFO (*3*), an FAD hydroquinone intervenes in order to reduce the transiently formed exocyclic methylene intermediate on the C5-U54. Therefore, the catalytic methylating intermediate identified in $TrmFO_{BS}$ must contain, in addition to CH_2THF, a two electron-reduced flavin. From the optical spectrum (Figure 2), several FAD redox states appear to exist in the protein: FAD_{ox}, FADH• and at least another species showing maximum absorption at 380 nm. Interestingly, the ferricyanide-treated enzyme, which has lost FADH• (Figure 6), can still methylate efficiently tRNA. Therefore, the air-stable FADH• cannot serve as an electron donor in the methylation reaction and it is unlikely that disproportionation of FADH• into an FAD hydroquinone is responsible for the catalytic activity of freshly purified $TrmFO_{BS.}$. Consequently, the catalytic intermediate is likely a flavin hydroquinone,

which appears to be well insulated in the active site of $TrmFO_{BS}$ and thus inaccessible to oxidation by ferricyanide.

After ferricyanide treatment, the enzyme conserves a high peak centered at 380 nm and a poorly resolved line shape below 340 nm (Figure 6). Assuming that these optical features are due to a mixture of FAD_{ox} and unknown FAD derivative, the spectrum of this latter component was calculated from the ferricyanide-treated $TrmFO_{BS}$ by subtracting the contribution of oxidized flavin (Figure 6). The resulting spectrum is consistent with that of the fluorescence excitation spectrum obtained at λ_{em} 450 nm, indicating that both absorption and fluorescence spectra identified the same flavin species (Figure 6, 7A). In addition to the peak with a maximum at 380 nm, the unknown FAD species exhibits a small additional peak at ~320 nm (Figure 6). This spectrum could neither be attributed to the FAD•- nor to the FADH• radical. Instead, it clearly shares some similarity with the spectra of C4α-FAD-cysteinyl adducts (*35-37*). In consequence, the calculated absorption spectrum could account for two reduced flavin forms instead of one, notably a hydroquinone present in the catalytic intermediate and an inactive C4α adduct covalently linked to the nearby reactive Cys53. Nonetheless, the existence of a C4α adduct with $TrmFO_{BS}$ is not settled yet. Indeed, exposition of fully oxidized $TrmFO_{BS}$ to UV-light did not generate the 380 nm peak (data not shown), as is most often the case with flavoproteins that are capable to form C4α-cysteinyl adducts (*35-37*). In addition, the cysteinyl flavin adducts are usually not fluorescent, in contrast to the 380 nm absorbing species in $TrmFO_{BS}$.

Alternatively, the uncommon shape of the calculated spectrum could originate from an FAD hydroquinone located in a particular environment, resulting from the

stacking of the isoalloxazine ring with CH_2THF. Actually, adding formaldehyde to freshly purified $TrmFO_{BS}$ to shift the equilibrium toward CH_2THF formation leads to significant spectral changes, notably an enlargement of both the 380 nm and FADH• bands (Figure 9B). These particular spectral changes may arise from a charge transfer between a positive charge and a flavin hydroquinone, which could also explain the unusual stretched peak between 550 and 650 nm observed in the freshly purified enzyme. Generally, enzymes that bind CH_2THF activate this folate derivative by inducing an acid-catalyzed opening of the imidazolidine ring, which generates a 5-iminium cation intermediate (*38-41*). Thus, a charge transfer could take place between this latter and a pre-reduced flavin hydroquinone in $TrmFO_{BS}$.

Flavoenzymes exhibit a large variation in their air-oxidation reaction rate constants, ranging from 10^6 (diffusion-controlled rate) to 2 $M^{-1}.s^{-1}$ (observed for flavocytochrome *c*) (*9*). Thermodynamic factors are often insufficient to account for the presence of normally unstable intermediates (*9, 42*). Actually, several flavoproteins such as dihydroorotate dehydrogenase (*43*) or mammalian medium-chain acyl-coenzyme A dehydrogenase (*44*) had their oxygen reactivity seriously altered by substrate binding. It was suggested that ligand binding had increased the redox potential of the flavin and induced a complete desolvation of the active site. It is likely that the stabilization of the reduced flavin in $TrmFO_{BS}$ originates from the presence of the CH_2THF substrate, trapped in the enzyme active site. The degradation of CH_2THF may relieve the initially buried cofactor to solvent. Oxygen would then have access to the $TrmFO_{BS}$ reduced flavin forms and oxidize them instantly (Figure 9A). Accordingly, CH_2THF decomposition into THF and formaldehyde could be the rate-limiting step in the

oxidation of reduced flavins (Figure 8). The rate constant for FAD hydroquinone oxidation by molecular oxygen is much higher than that observed for the air-stable reduced forms. Hence, our present results suggest that sequestered CH_2THF acts as a protecting agent of the highly reactive reduced flavins, keeping the active site away from uncoupled reactions.

The FAD reduced forms have probably been kinetically trapped inside the active site of $TrmFO_{BS}$. The fundamental question as to whether the FADH• and the air-stable catalytic FAD reduced form are thermodynamically relevant was answered by reductive anaerobic titration of oxidized $TrmFO_{BS}$ (Figure 9A). Surprisingly, no formation of FADH• radical was detected either during the reductive titration with dithionite or the oxidative titration of the fully reduced $TrmFO_{BS}$ with oxidized $TrmFO_{BS}$ or ferricyanide (data not shown). Instead, a steady transition between oxidized FAD and an extremely air-sensitive hydroquinone was observed, ruling out a thermodynamic stabilization of both FADH• and the catalytically competent FAD form. Therefore, the existence of the FADH• radical in freshly purified $TrmFO_{BS}$ cannot be accounted for by the known dismutation reaction between oxidized and reduced flavin ($FAD + FADH_2 \Leftrightarrow 2\ FADH•$). Since the TrmFO reaction proceeds via a hydride transfer rather than a radical mechanism (*3*), it is probable that FADH• is generated by partial air-oxidation of the air-stable hydroquinone during the purification process and that the FADH• redox state has no physiological relevance. Our present thermodynamic data suggest that accumulation of the air-stable FADH• and catalytic intermediate containing both reduced FAD and methyl donor, observed during the purification of $TrmFO_{BS}$, results from kinetic trapping, presumably driven by protein conformational changes.

Acknowledgements

We thank Dr R. Moser, Merck-Eprova, AG, Switzerland, for providing the folate derivatives; Michael C. Marden and Laurent Kiger for providing access to anaerobic devices, Sylvie Auxilien, Hannu Myllykallio and Florence Lederer for helpful discussions.

References

1. Motorin, Y., and Helm, M. (2010) tRNA stabilization by modified nucleotides, *Biochemistry 49*, 4934-4944.
2. Delk, A. S., Nagle, D. P., Jr., Rabinowitz, J. C., and Straub, K. M. (1979) The methylenetetrahydrofolate-mediated biosynthesis of ribothymidine in the transfer-RNA of *Streptococcus faecalis*: incorporation of hydrogen from solvent into the methyl moiety, *Biochem Biophys Res Commun 86*, 244-251.
3. Delk, A. S., Nagle, D. P., Jr., and Rabinowitz, J. C. (1980) Methylenetetrahydrofolate-dependent biosynthesis of ribothymidine in transfer RNA of *Streptococcus faecalis*. Evidence for reduction of the 1-carbon unit by FADH2, *J Biol Chem 255*, 4387-4390.
4. Urbonavicius, J., Skouloubris, S., Myllykallio, H., and Grosjean, H. (2005) Identification of a novel gene encoding a flavin-dependent tRNA:m^5U methyltransferase in bacteria - evolutionary implications, *Nucleic Acids Res 33*, 3955-3964.
5. Nishimasu, H., Ishitani, R., Yamashita, K., Iwashita, C., Hirata, A., Hori, H., and Nureki, O. (2009) Atomic structure of a folate/FAD-dependent tRNA T54 methyltransferase, *Proc Natl Acad Sci U S A 106*, 8180-8185.
6. Payne, G., Heelis, P. F., Rohrs, B. R., and Sancar, A. (1987) The active form of *Escherichia coli* DNA photolyase contains a fully reduced flavin and not a flavin radical, both in vivo and in vitro, *Biochemistry 26*, 7121-7127.

7. Gutierrez, A., Lian, L. Y., Wolf, C. R., Scrutton, N. S., and Roberts, G. C. (2001) Stopped-flow kinetic studies of flavin reduction in human cytochrome P450 reductase and its component domains, *Biochemistry 40*, 1964-1975.

8. Hanley, S. C., Ost, T. W., and Daff, S. (2004) The unusual redox properties of flavocytochrome P450 BM3 flavodoxin domain, *Biochem Biophys Res Commun 325*, 1418-1423.

9. Mattevi, A. (2006) To be or not to be an oxidase: challenging the oxygen reactivity of flavoenzymes, *Trends Biochem Sci 31*, 276-283.

10. Hamdane, D., Skouloubris, S., Myllykallio, H., and Golinelli-Pimpaneau, B. (2010) Expression and purification of untagged and histidine-tagged folate-dependent tRNA:m(5)U54 methyltransferase from *Bacillus subtilis*, *Protein Expr Purif 73*, 83-89.

11. Un, S., Dorlet, P., and Rutherford, A. W. (2001) A high-field EPR tour of radicals in photosystems I and II *Appl.Magn.Reson. 21*, 341-361.

12. Grosjean, H., Droogmans, L., Roovers, M., and Keith, G. (2007) Detection of enzymatic activity of transfer RNA modification enzymes using radiolabeled tRNA substrates, *Methods Enzymol 425*, 55-101.

13. Massey, V., and Palmer, G. (1966) On the existence of spectrally distinct classes of flavoprotein semiquinones. A new method for the quantitative production of flavoprotein semiquinones, *Biochemistry 5*, 3181-3189.

14. Okafuji, A., Schnegg, A., Schleicher, E., Mobius, K., and Weber, S. (2008) g-tensors of the flavin adenine dinucleotide radicals in glucose oxidase: a

comparative multifrequency electron paramagnetic resonance and electron-nuclear double resonance study, *J Phys Chem B 112*, 3568-3574.

15. Barquera, B., Morgan, J. E., Lukoyanov, D., Scholes, C. P., Gennis, R. B., and Nilges, M. J. (2003) X- and W-band EPR and Q-band ENDOR studies of the flavin radical in the Na^+ -translocating NADH:quinone oxidoreductase from *Vibrio cholerae*, *J Am Chem Soc 125*, 265-275.

16. Schleicher, E., Wenzel, R., Ahmad, M., Batschauer, A., Essen, L. O., Hitomi, K., Getzoff, E. D., Bittl, R., Weber, S., and Okafuji, A. (2010) The Electronic State of Flavoproteins: Investigations with Proton Electron–Nuclear Double Resonance, *Applied Magnetic Resonance 37*, 339-352.

17. Kay, C. W., Bittl, R., Bacher, A., Richter, G., and Weber, S. (2005) Unambiguous determination of the g-matrix orientation in a neutral flavin radical by pulsed electron-nuclear double resonance at 94 GHz, *J Am Chem Soc 127*, 10780-10781.

18. Schleicher, E., Hitomi, K., Kay, C. W., Getzoff, E. D., Todo, T., and Weber, S. (2007) Electron nuclear double resonance differentiates complementary roles for active site histidines in (6-4) photolyase, *J Biol Chem 282*, 4738-4747.

19. Hitomi, K., Kim, S. T., Iwai, S., Harima, N., Otoshi, E., Ikenaga, M., and Todo, T. (1997) Binding and catalytic properties of *Xenopus* (6-4) photolyase, *J Biol Chem 272*, 32591-32598.

20. Usman, A., Brazard, J., Martin, M. M., Plaza, P., Heijde, M., Zabulon, G., and Bowler, C. (2009) Spectroscopic characterization of a (6-4) photolyase from the green alga *Ostreococcus tauri*, *J Photochem Photobiol B 96*, 38-48.

21. Li, J., Uchida, T., Ohta, T., Todo, T., and Kitagawa, T. (2006) Characteristic structure and environment in FAD cofactor of (6-4) photolyase along function revealed by resonance Raman spectroscopy, *J Phys Chem B 110*, 16724-16732.

22. Bradley, L. H., and Swenson, R. P. (1999) Role of glutamate-59 hydrogen bonded to N(3)H of the flavin mononucleotide cofactor in the modulation of the redox potentials of the *Clostridium beijerinckii* flavodoxin. Glutamate-59 is not responsible for the pH dependency but contributes to the stabilization of the flavin semiquinone, *Biochemistry 38*, 12377-12386.

23. Biskup, T., Schleicher, E., Okafuji, A., Link, G., Hitomi, K., Getzoff, E. D., and Weber, S. (2009) Direct observation of a photoinduced radical pair in a cryptochrome blue-light photoreceptor, *Angew Chem Int Ed Engl 48*, 404-407.

24. Schleicher, E., Bittl, R., and Weber, S. (2009) New roles of flavoproteins in molecular cell biology: blue-light active flavoproteins studied by electron paramagnetic resonance, *FEBS J 276*, 4290-4303.

25. Un, S., and Sedoud, A. (2010) High-field EPR Study of the Effect of Chloride on Mn2+ Ions in Frozen Aqueous Solutions *App. Mag. Res. 37*, 247-256.

26. Johnson, J. L., Hamm-Alvarez, S., Payne, G., Sancar, G. B., Rajagopalan, K. V., and Sancar, A. (1988) Identification of the second chromophore of *Escherichia coli* and yeast DNA photolyases as 5,10-methenyltetrahydrofolate, *Proc Natl Acad Sci U S A 85*, 2046-2050.

27. Scrima, A., Vetter, I. R., Armengod, M. E., and Wittinghofer, A. (2005) The structure of the TrmE GTP-binding protein and its implications for tRNA modification, *EMBO J 24*, 23-33.

28. Cook, R. J., and Wagner, C. (1986) Purification of rat liver folate-binding protein: cytosol I, *Methods Enzymol 122*, 251-255.

29. Schirch, V., and Strong, W. B. (1989) Interaction of folylpolyglutamates with enzymes in one-carbon metabolism, *Arch Biochem Biophys 269*, 371-380.

30. Kim, D. W., Huang, T., Schirch, D., and Schirch, V. (1996) Properties of tetrahydropteroylpentaglutamate bound to 10-formyltetrahydrofolate dehydrogenase, *Biochemistry 35*, 15772-15783.

31. Knighton, D. R., Kan, C. C., Howland, E., Janson, C. A., Hostomska, Z., Welsh, K. M., and Matthews, D. A. (1994) Structure of and kinetic channelling in bifunctional dihydrofolate reductase-thymidylate synthase, *Nat Struct Biol 1*, 186-194.

32. Trujillo, M., Donald, R. G., Roos, D. S., Greene, P. J., and Santi, D. V. (1996) Heterologous expression and characterization of the bifunctional dihydrofolate reductase-thymidylate synthase enzyme of *Toxoplasma gondii*, *Biochemistry 35*, 6366-6374.

33. Pawelek, P. D., Allaire, M., Cygler, M., and MacKenzie, R. E. (2000) Channeling efficiency in the bifunctional methylenetetrahydrofolate dehydrogenase/cyclohydrolase domain: the effects of site-directed mutagenesis of NADP binding residues, *Biochim Biophys Acta 1479*, 59-68.

34. Pejchal, R., Sargeant, R., and Ludwig, M. L. (2005) Structures of NADH and CH_3-H4folate complexes of *Escherichia coli* methylenetetrahydrofolate reductase reveal a spartan strategy for a ping-pong reaction, *Biochemistry 44*, 11447-11457.

35. Miller, S. M., Massey, V., Ballou, D., Williams, C. H., Jr., Distefano, M. D., Moore, M. J., and Walsh, C. T. (1990) Use of a site-directed triple mutant to trap intermediates: demonstration that the flavin C(4a)-thiol adduct and reduced flavin are kinetically competent intermediates in mercuric ion reductase, *Biochemistry 29*, 2831-2841.

36. Salomon, M., Christie, J. M., Knieb, E., Lempert, U., and Briggs, W. R. (2000) Photochemical and mutational analysis of the FMN-binding domains of the plant blue light receptor, phototropin, *Biochemistry 39*, 9401-9410.

37. Zoltowski, B. D., Schwerdtfeger, C., Widom, J., Loros, J. J., Bilwes, A. M., Dunlap, J. C., and Crane, B. R. (2007) Conformational switching in the fungal light sensor Vivid, *Science 316*, 1054-1057.

38. Sumner, J. S., and Matthews, R. G. (1992) Stereochemistry and mechanism of hydrogen transfer between NADPH and methylenetetrahydrofolate in the reaction catalyzed by methylenetetrahydrofolate reductase from pig liver, *J Am Chem Soc 114* 6949–6956.

39. Carreras, C. W., and Santi, D. V. (1995) The catalytic mechanism and structure of thymidylate synthase, *Annu Rev Biochem 64*, 721-762.

40. Perry, K. M., Carreras, C. W., Chang, L. C., Santi, D. V., and Stroud, R. M. (1993) Structures of thymidylate synthase with a C-terminal deletion: role of the C-terminus in alignment of 2'-deoxyuridine 5'-monophosphate and 5,10-methylenetetrahydrofolate, *Biochemistry 32*, 7116-7125.

41. Trimmer, E. E., Ballou, D. P., Galloway, L. J., Scannell, S. A., Brinker, D. R., and Casas, K. R. (2005) Aspartate 120 of *Escherichia coli* methylenetetrahydrofolate

reductase: evidence for major roles in folate binding and catalysis and a minor role in flavin reactivity, *Biochemistry 44*, 6809-6822.

42. Massey, V. (1994) Activation of molecular oxygen by flavins and flavoproteins, *J Biol Chem 269*, 22459-22462.

43. Palfey, B. A., Bjornberg, O., and Jensen, K. F. (2001) Insight into the chemistry of flavin reduction and oxidation in *Escherichia coli* dihydroorotate dehydrogenase obtained by rapid reaction studies, *Biochemistry 40*, 4381-4390.

44. Wang, R., and Thorpe, C. (1991) Reactivity of medium-chain acyl-CoA dehydrogenase toward molecular oxygen, *Biochemistry 30*, 7895-7901.

Tables

Table 1A. g-values and hyperfine couplings used to simulate the 285 GHz EPR spectrum of $TrmFO_{BS}$ FADH•. Δg is the Gaussian distribution in g-values used in the simulations. Hyperfine couplings are absolute values and given in MHz. Assignments were based on references (*14*) and (*15*).

Direction	g	Δg	A[N(5)]	A[N(10)]	A[H(5)]
g_x	2.00504	0.00027	25	0	39
g_y	2.00441	0.00016	16	0	0
g_z	2.00258	0.00012	45	27	27

Table 1B. Measured and calculated g-values for FADH• radicals.

	g_x	g_y	g_z	g_{iso}
		TrmFO		
Neutral	2.00504	2.00441	2.00258	2.00388
		NADH:quinone oxidoreductase[a]		
Neutral	2.00425	2.00360	2.00227	2.00355
Anion	2.00436	2.00402	2.00228	2.00337
		Glucose Oxidase[b]		
Neutral	2.0043	2.0036	2.0021	2.0035
Anion	2.00429	2.00389	2.00216	2.00345
		B3LYP/6-31+ G(D,P)		
		ε=20/H_2O hydrogen bond between a thiol group and N(5)H		
Neutral	2.00440	2.00371	2.00202	2.00338

[a] see (*15*)
[b] see (*14*)

Figure legends

Scheme 1: Molecular structures of oxidized FAD, (N(1)-deprotonated) hydroquinone $FADH^-$ and neutral (N(5)-protonated) FADH•, with the orientation of the g-tensors.

Figure 1: **A** Enzymatic reaction catalyzed by TrmFO (CH_2THF: 5,10 methylenetetrahydrofolate; THF: tetrahydrofolate; FAD: flavin adenine dinucleotide; $FADH_2$: hydroquinone; FAD_{ox}: fully oxidized FAD. **B** Structure of the active of $TrmFO_{TT}$ in complex with FAD (indicated in yellow) and tetrahydrofolate (indicated in red). The THF pteridin ring is sandwiched between the imidazole side-chain of His308 and the FAD isoalloxazine ring, whereas its NA2 atom is hydrogen bonded to the main-chain carbonyl of Arg309 and the Oδ1 atom of Asn310.

Figure 2: Optical absorption spectrum of $TrmFO_{BS}$ in 50 mM sodium phosphate, pH 8 just after the purification (continuous line) and after air oxidation for 20h (dashed line).

Figure 3: The 285 GHz EPR (A) and 95 GHz ENDOR (B) spectra of the $TrmFO_{BS}$ FADH• radical. **A** The g_{eff} values on the upper horizontal scale correspond to the positions of three of the six sharp resonances of the manganese Mn:MgO g-standard, the dashed vertical lines mark the three principle g-values of the radical and the solid line the free electron g-value (2.00232). The dashed trace overlaying the spectrum is a simulation (see Experimental Procedures for details and Table 1 for spin parameters used). The arrow marks the approximate position in g-value, where the 95 GHz ENDOR spectrum was obtained.

Figure 4: Kinetic and stoichiometry of the tRNA methylation reaction catalyzed by

$TrmFO_{BS}$. **A** Time course for the methylation of U54 in *E.coli* $tRNA^{Asp}$ by $TrmFO_{BS}$ in the absence of NAD(P)H and CH_2THF. **B** MALDI mass spectrometry analysis of methylated $tRNA^{Asp}$ formed after 1 h incubation at 37°C of *E. coli* $tRNA^{Asp}$ with $TrmFO_{BS}$ and digestion by RNase A. The main spectrum and lower insert shows tRNA from the control sample that was not incubated with enzyme. The two upper inserts (with tRNA and TrmFO in 1:10 and 1:1 ratios) correspond to the spectral region around the 1705.2 fragment, which contains the target uridine, to show the peaks for the nonmethylated (*m/z* 1705.2) and the corresponding monomethylated (*m/z* 1719.2) ions.

Figure 5: MALDI Mass spectrum in positive mode of the small molecules released from $TrmFO_{BS}$ after acidic treatment under anaerobic conditions (see experimental procedures). The upper panel shows the spectrum of free commercial oxidized FAD (theoretical mass of 785.16), treated in the same conditions as $TrmFO_{BS}$. The middle panel represents the spectrum of the reaction mixture of the FAD hydroquinone with methyliodide in anaerobic conditions and treated as $TrmFO_{BS}$. The presence of methylated FAD (theoretical mass of 789.16) is evidenced by the peak envelope starting at m/*z* of 800.14. The lower panel shows the molecule isolated from $TrmFO_{BS}$.

Figure 6: Optical absorption spectrum of freshly purified $TrmFO_{BS}$ (~ 18 μM) after treatment with 10-fold molar excess of ferricyanide (black curve). The calculated spectrum of the species absorbing at 380 nm (red curve) was obtained after substracting the contribution of FAD_{ox} (grey curve) from the spectrum of the ferricyanide-treated $TrmFO_{BS}$ (black curve). Solution is unique if one assumes that this species must exhibit a

positive absorbance at all wavelengths and should not possess the absorption maximum at ~480 nm as does oxidized FAD. The inset is an estimate of the extinction coefficient of the calculated flavin species.

Figure 7: Steady state fluorescence spectra of freshly purified $TrmFO_{BS}$ **(A)** and after denaturation in 100 mM sodium phosphate buffer at pH 8 containing 8 M urea **(B)**. The final concentration of wild type $TrmFO_{BS}$ was ~ 3 to 4 μM. The dashed lines are the excitation spectra recorded at a λ_{em}=528 nm (blue) and at λ_{em}=450 nm (red), whereas the continuous lines are the emission spectra recorded at λ_{ex}=450 nm (blue) and at λ_{ex}=370 nm (red). Upon excitation at 450 nm, the quantum yield of the emission peak at 528 nm characteristic of FAD_{ox} was 0.015 i. e. ~ 5 % that of free oxidized FAD.

Figure 8: Decay Kinetics of the air-stable flavin species in $TrmFO_{BS}$ at pH 8. **A** Variation of the absorbance spectrum of $TrmFO_{BS}$ upon air oxidation. **B** Increase of the absorbance at 450 nm (upper panel) and decrease of the absorbance at 595 nm (lower panel) as function of time in the presence of O_2 (1 atm, circles; 80 μM, squares) and 10 mM formaldehyde (triangles). The normalized kinetics traces at 595 and 445 nm were fitted to mono-exponential $\Delta A_N^{595}(t) = \exp(-kt)$.

Figure 9: A Anaerobic titration of 10 μM oxidized $TrmFO_{BS}$ in 50 mM sodium phosphate pH 8 by dithionite. The sample was equilibrated for 5 min after each addition of sodium dithionite solution before recording the spectrum. **B** Optical absorption spectrum of $TrmFO_{BS}$ in 50 mM potassium phosphate, 150 mM NaCl, 10% glycerol at

pH 8, just after the purification (green line), after addition of 10 mM formaldehyde (red line) and subsequent air oxidation for 12h (black line). The final spectrum of oxidized $TrmFO_{BS}$ is shown in blue.

Scheme 1

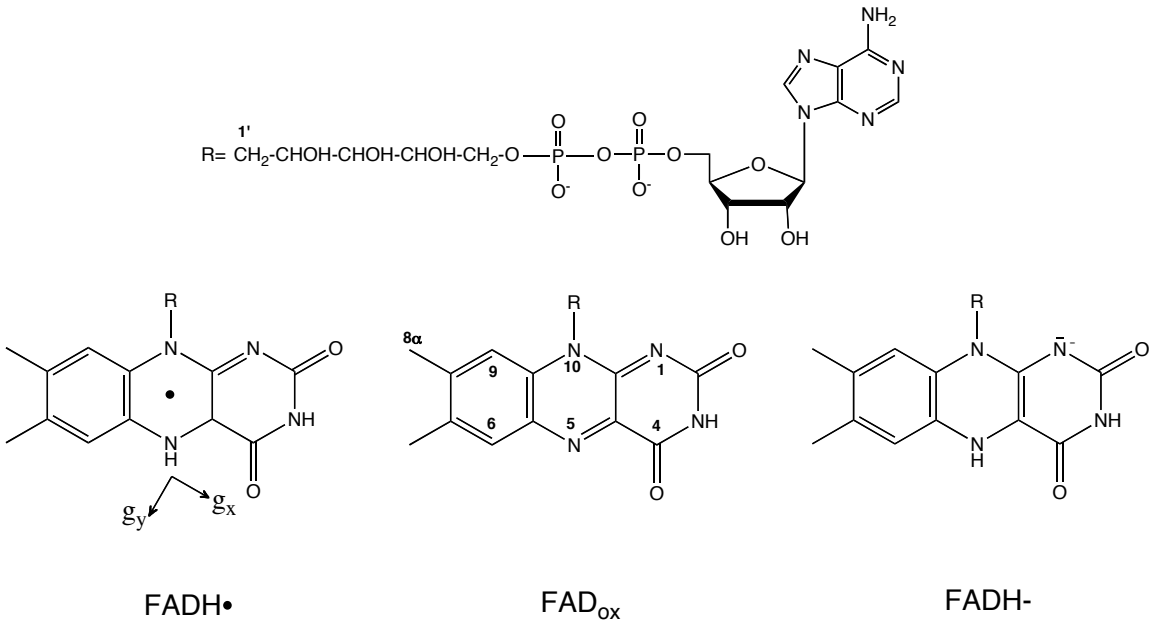

FADH• FAD_{ox} FADH-

g_z is orientated perpendicular to the FADH• isoalloxazine plane.

Figures

Figure 1

A

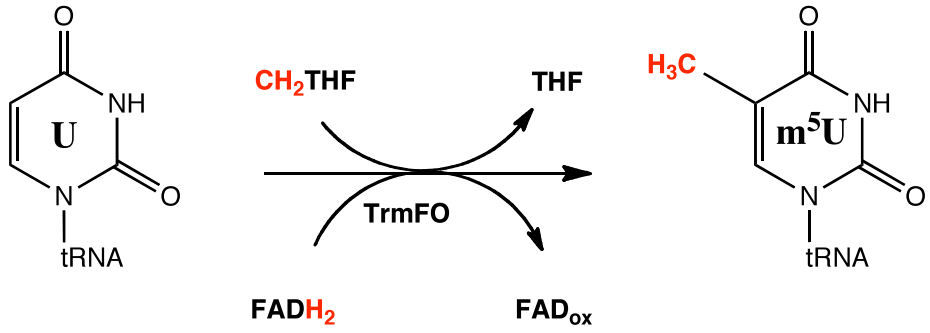

B

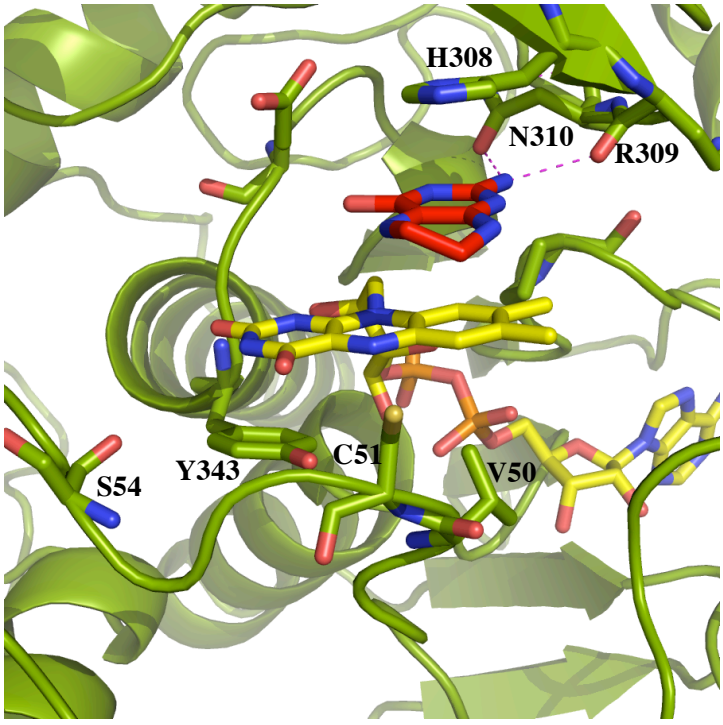

Figure 2

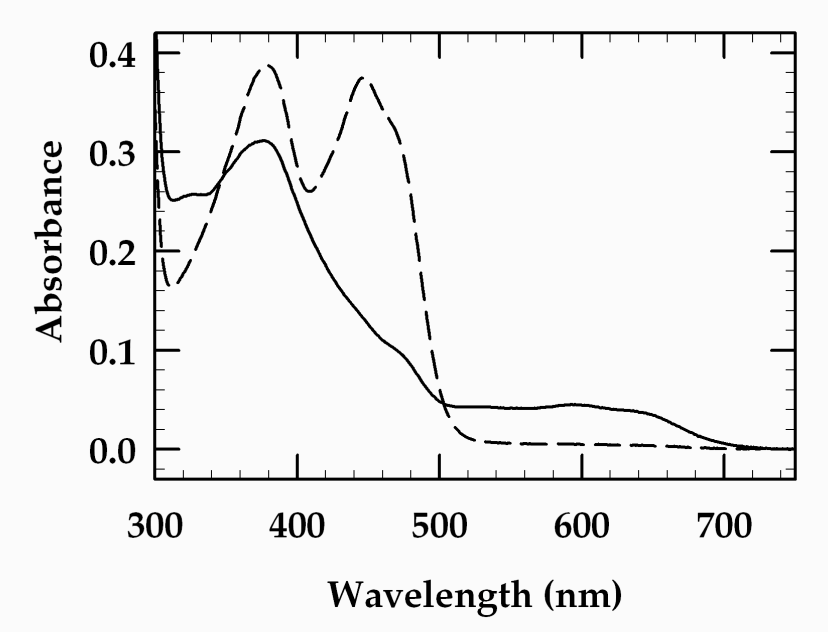

Figure 3

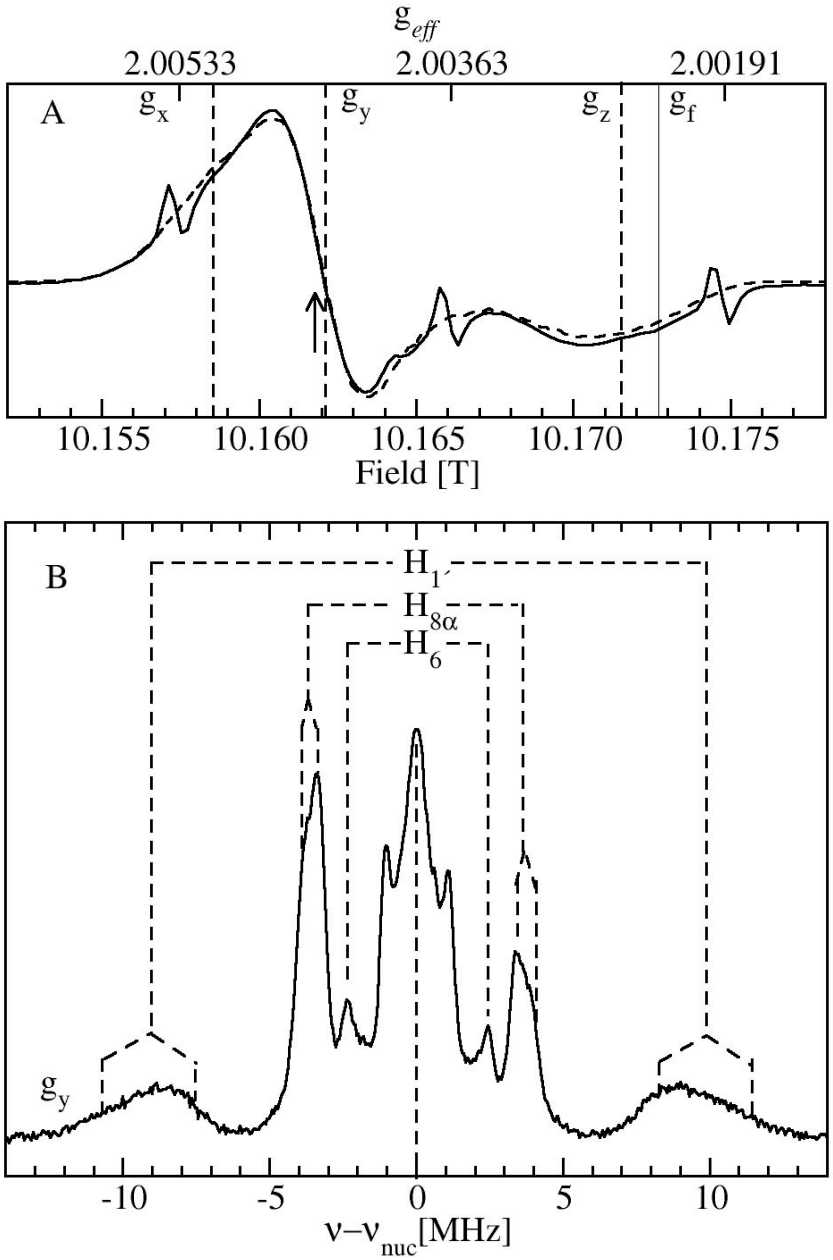
g_eff
2.00533
2.00363
2.00191
A
g_x
g_y
g_z
g_f
10.155
10.160
10.165
10.170
10.175
Field [T]
B
H_1´
H_8α
H_6
g_y
-10
-5
0
5
10
ν–ν_nuc[MHz]

Figure 4

A

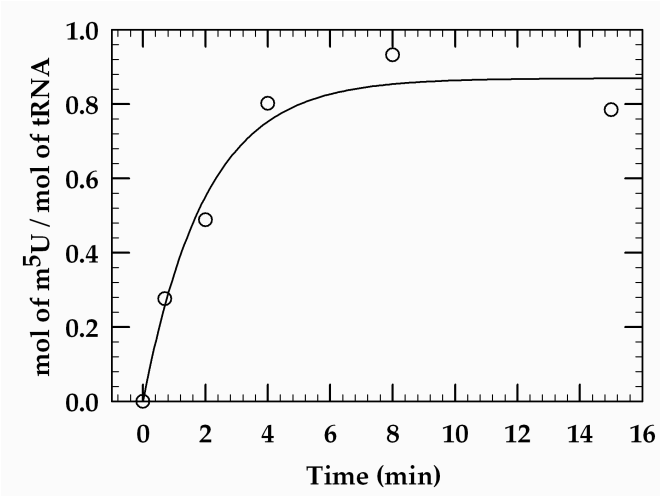
mol of m5U / mol of tRNA
1.0
0.8
0.6
0.4
0.2
0.0
0
2
4
6
8
10
12
14
16
Time (min)

B

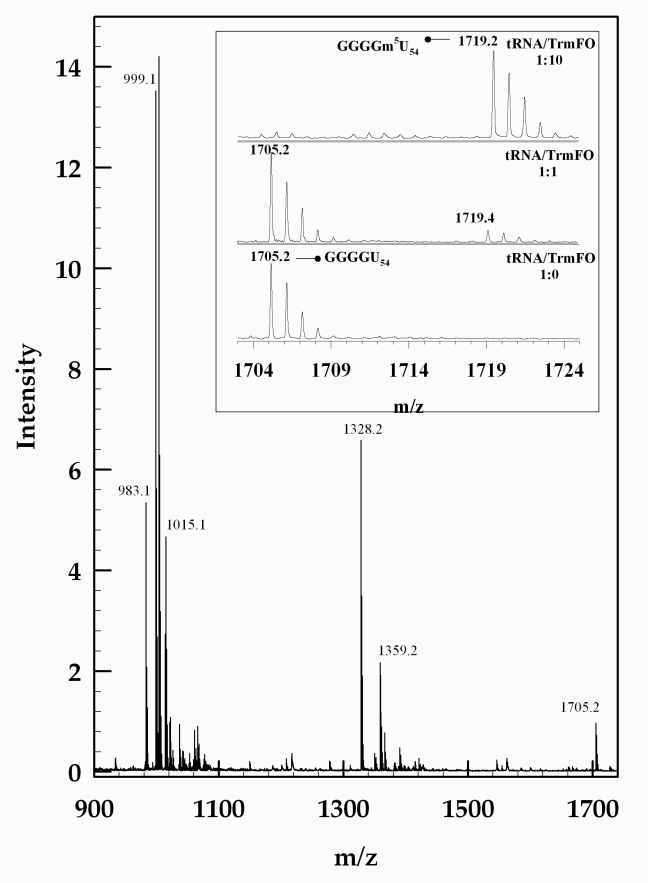
Intensity
14
12
10
8
6
4
2
0
900
1100
1300
1500
1700
m/z
999.1
983.1
1015.1
1328.2
1359.2
1705.2
GGGGm5U54
1719.2
tRNA/TrmFO
1:10
1705.2
tRNA/TrmFO
1:1
1719.4
1705.2
GGGGU54
tRNA/TrmFO
1:0
1704
1709
1714
1719
1724
m/z

Figure 5

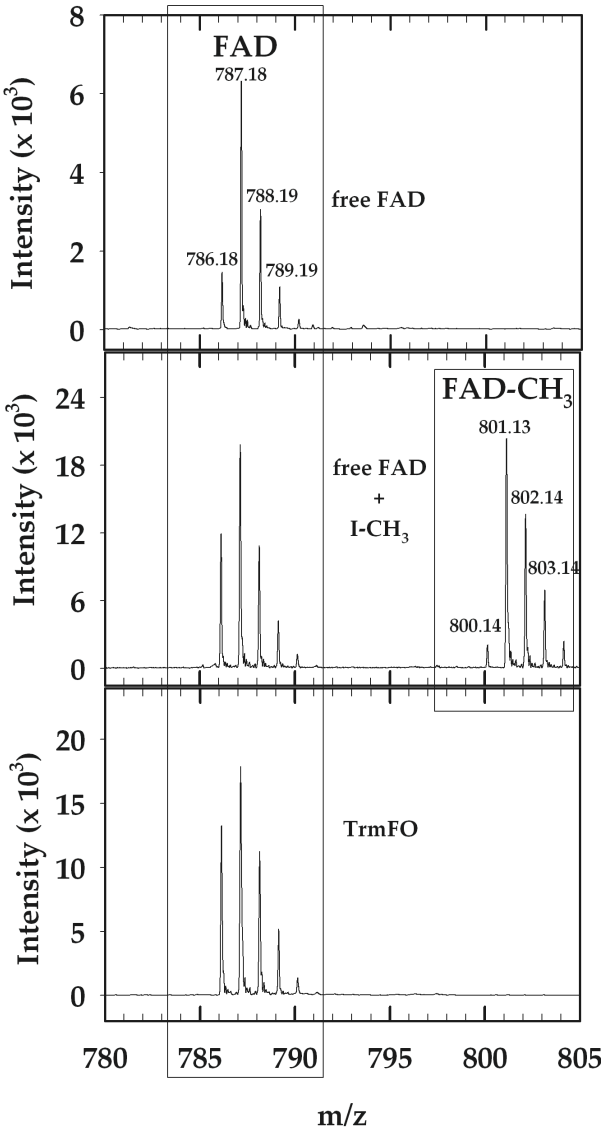
FAD
787.18
788.19
786.18
789.19
free FAD
Intensity (x 10^3)
FAD-CH3
801.13
802.14
803.14
800.14
free FAD
+
I-CH3
TrmFO
m/z
780
785
790
795
800
805

Figure 6

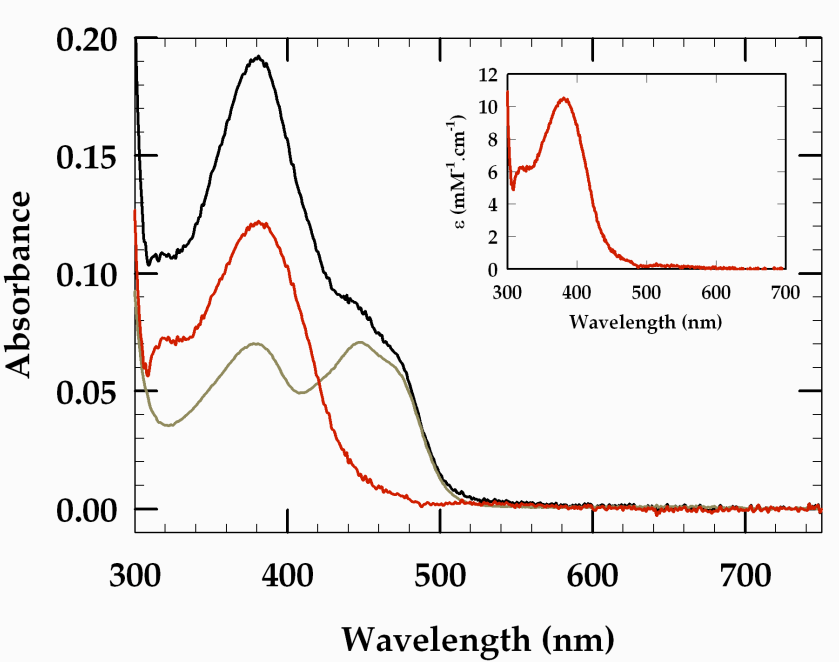
Absorbance
0.20
0.15
0.10
0.05
0.00
300
400
500
600
700
Wavelength (nm)
ε (mM-1.cm-1)
12
10
8
6
4
2
0
300
400
500
600
700
Wavelength (nm)

Figure 7

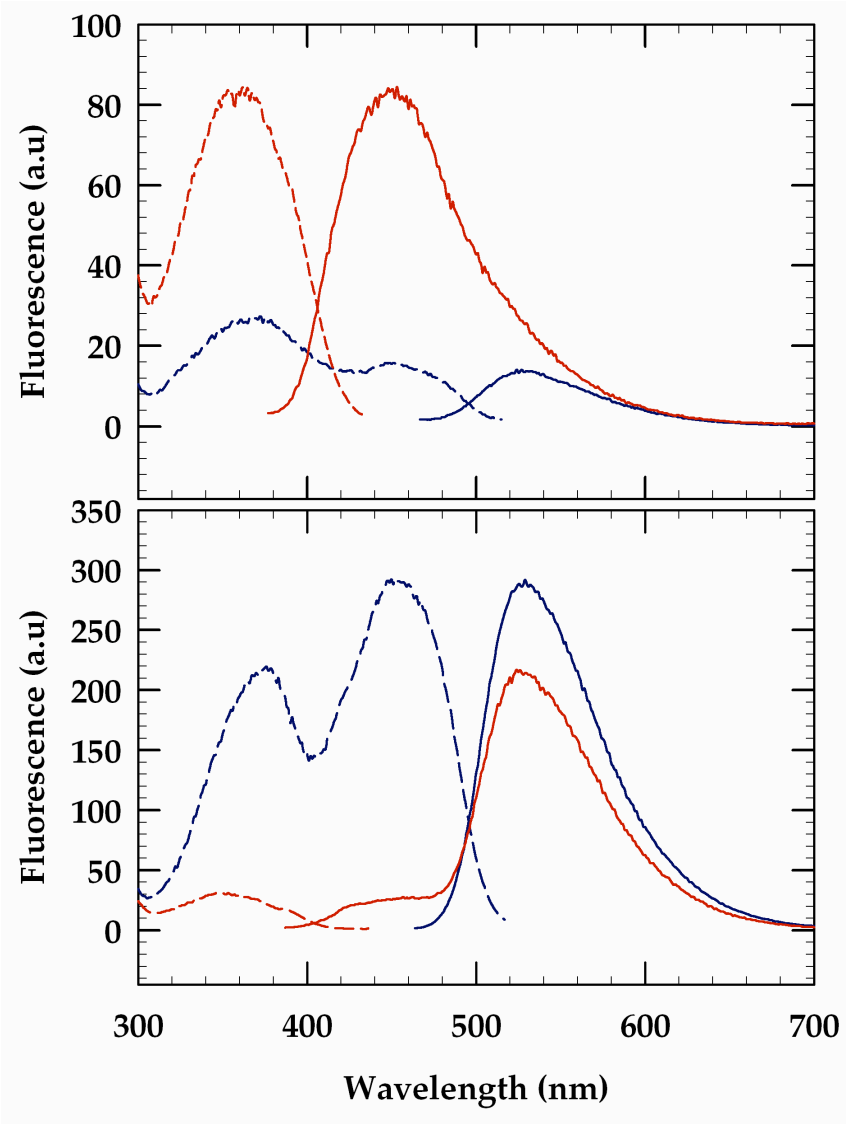
A
B
Fluorescence (a.u)
Fluorescence (a.u)
100
80
60
40
20
0
350
300
250
200
150
100
50
0
300
400
500
600
700
Wavelength (nm)

Figure 8

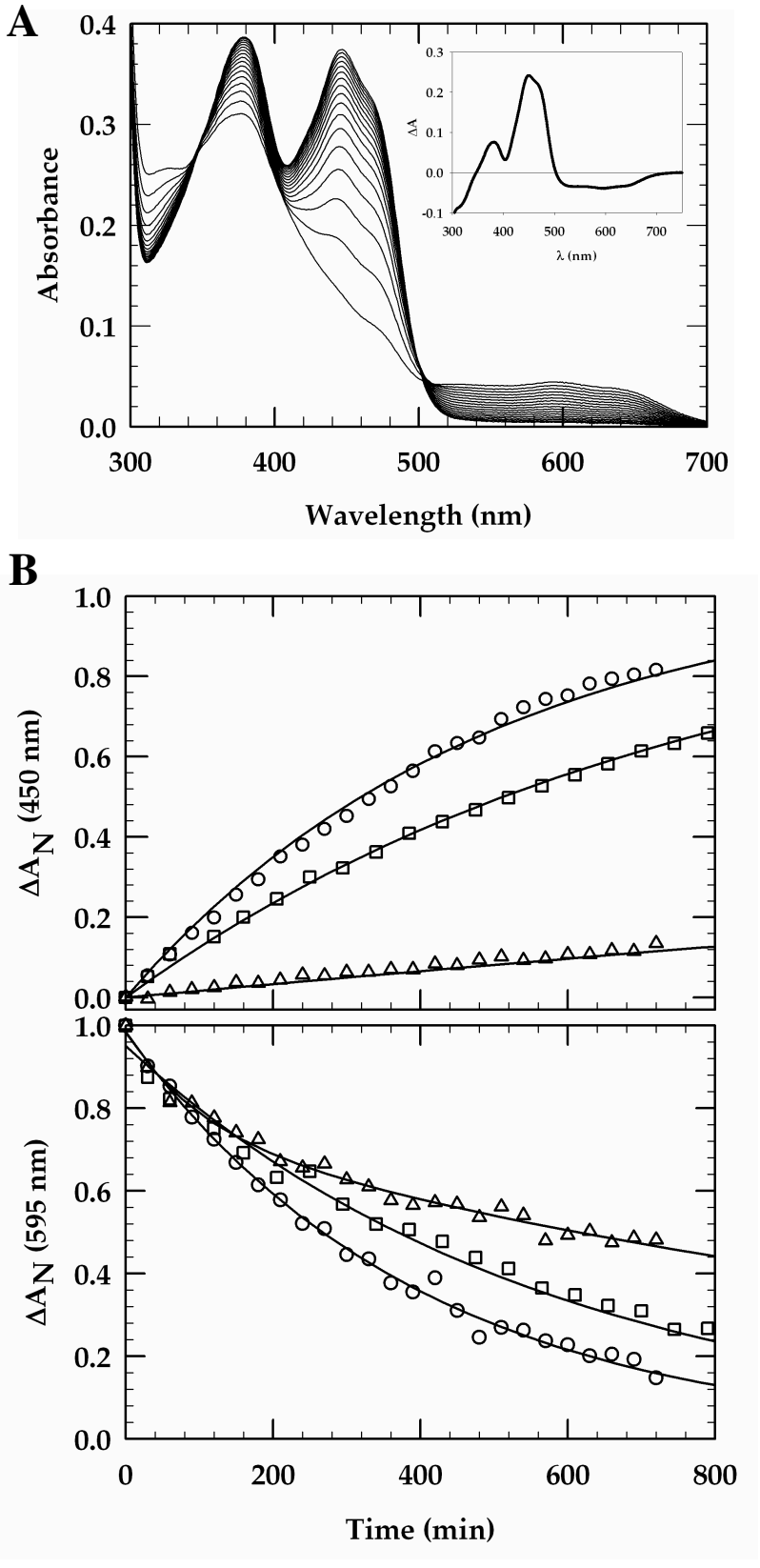
A
Absorbance
Wavelength (nm)
ΔA
λ (nm)
B
ΔA_N (450 nm)
ΔA_N (595 nm)
Time (min)

Figure 9

A

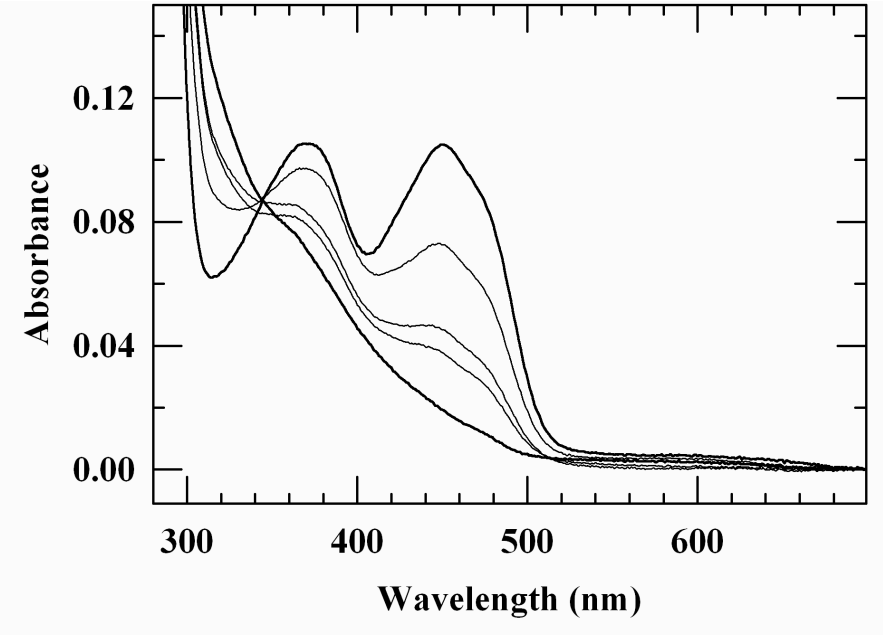
0.12
0.08
0.04
0.00
Absorbance
300
400
500
600
Wavelength (nm)

B

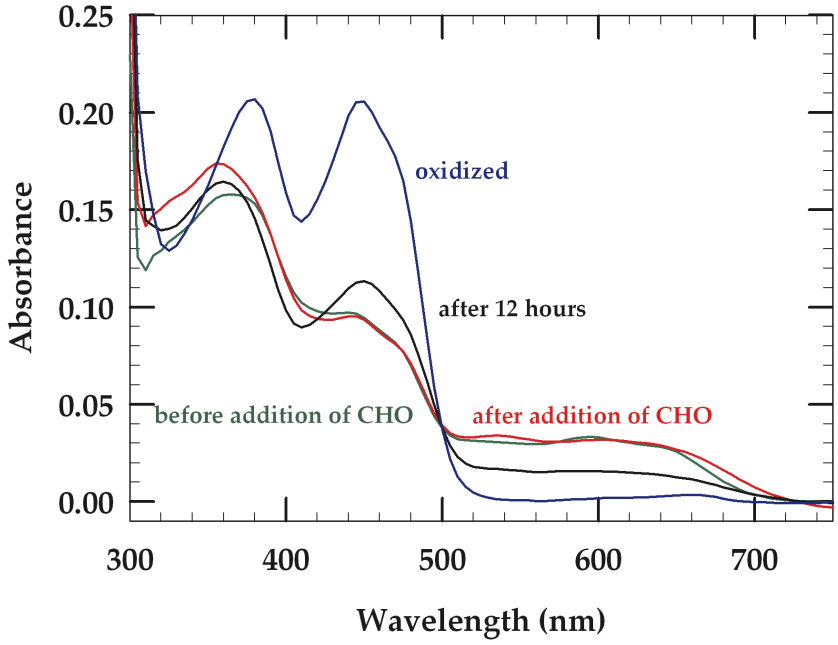
0.25
0.20
0.15
0.10
0.05
0.00
Absorbance
oxidized
after 12 hours
before addition of CHO
after addition of CHO
300
400
500
600
700
Wavelength (nm)

For Table of contents use only

A Catalytic Intermediate and Several Flavin Redox States Stabilized by Folate-Dependent tRNA Methyltransferase from *Bacillus subtilis*.

Djemel Hamdane, Vincent Guérineau, Sun Un and Béatrice Golinelli-Pimpaneau